ASSOCIAÇÃO BRASILEIRA DE ENERGIA NUCLEAR – ABEN
2019 International Nuclear Atlantic Conference - INAC 2019
Santos, SP, Brazil, October 21-25, 2019

Agência Brasileira do ISBN
ISBN 978-85-99141-08-3
9 788599 141083

PERFORMANCE ANALYSIS OF UO2-SiC FUEL UNDER NORMAL CONDITIONS

Daniel de Souza Gomes and Antonio Teixeira e Silva

Instituto de Pesquisas Energéticas e Nucleares (IPEN / CNEN - SP)
Av. Professor Lineu Prestes 2242
05508-000 São Paulo, SP, Brazil
dsgomes@ipen.br, teixeira@ipen.br

ABSTRACT

This study aims to investigate a fuel mixture of silicon carbide (SiC) and uranium dioxide (UO_2) and analyze performance when this fuel applies to light-water reactors (LWRs). Utilization of the licensing code, FRAPCON, with UO_2 helped to determine the fuel response under normal conditions initially. High thermal conductivity could permit the use of UO_2-10 vol% SiC fuel, showing thermal conductivity values that are far superior to the UO_2 alone, exceeding 50% at 900 °C. Ultimately, the formulation should reduce gaseous fission products, avoid fuel cracking, and improve safety margins. SiC has excellent physical properties such as chemical stability, a cross-section with low absorption, irradiation resistance, and a higher melting point. There are some benefits for fuels that use carbon composites such as UO_2-carbon nanotube (CNT), and UO_2-diamonds. The pellets containing fractions of the carbon limit the amount of fissile U-235 and require additional enrichment to produce the same energy. In the past, there have been various attempts to increase the thermal conductivity of UO_2. High conductivity is present in uranium nitride (UN), uranium carbide (UC), and UO_2 mixed with beryllium oxide (BeO). The production method of UO_2-SiC fuels should include the spark plasma sintering (SPS) technique. Advantages of SPS include a lower manufacturing temperature of 1050°C, better results, and reduced processing time of 30 s. SPS can help produce more tolerant fuels, such as UO_2-SiC, UO_2-carbon nanotube, and diamond powder dispersion in the UO_2 matrix. The thermal conductivity of SiC can decrease substantially under irradiation. UO_2-diamond has some drawbacks because of graphitization phenomena.

INTRODUCTION

Uranium dioxide is the most common fuel material used in nuclear power reactor fleets. Uranium dioxide has a low thermal conductivity of 2.8 W/m-K at 1000 °C. During regular reactor operation, after the densification phase, the thermal gradient into the pellet increases and induces the pellet cracking and relocations phenomena. These combined effects are undesirable features when considering risk management of the nuclear unit. The Fukushima disaster also prompted the start of accident tolerant fuel (ATF) initiatives.

The higher fuel temperatures trigger a series of problems, such as pellet swelling caused by fission gas bubbles and thermal expansion. Subsequently, the Fukushima accident in 2011 played an essential role in highlighting the weaknesses of uranium dioxide nuclear fuel. The ATF program started on an international campaign focused on promoting more tolerant fuels. The researchers on ATF initiatives focused on the intermediate stage between Gen-III and Gen-IV reactors [1].

1.1 Enhanced Thermal Conductivity Fuels

Using polymer infiltration pyrolysis (PIP) produced a ceramic composite of uranium oxide (U_3O_8) into a silicon carbide (SiC) matrix [2]. These experiments began with a series of pyrolysis processes and chemical interactions between U_3O_8 and SiC. Tests performed at higher rates of heat and pressure can produce composites of silicon carbide whiskers and uranium dioxide (UO_2) [3]. The spark plasma sintering (SPS) is a function of parameters such as current pulses of 3000 A, hold time, heat transfer rates, and a pressure of 40 MPa. Using SPS, uranium dioxide can sinter with the addition of carbon compounds [4]. Also, the SPS method could permit composite UO_2 matrices permeated with silicon carbide, carbon nanotube (CNT), or diamond powders. Pellet fuels with enhanced homogenization properties result from the result of the SPS method. Composites, such as UO_2-SiC, UO_2-CNT, and UO_2-graphene, all contain a higher thermal conductivity than UO_2, making them attractive as potential fuel combinations.

Initially, more tolerant fuels proposed to experiment based on matrices of uranium silicide (U3Si2), uranium nitride (UN), and uranium carbides (UC). Fuels fabricated have a higher fissile density such as UN, U_3Si_2, and UC. For the same volume of fuel, less fuel enrichment is necessary. It is essential to note the drawbacks with U_3Si_2, such as a higher swelling rate and a lower melting point than UO_2. Both the UN and UC fuels have reduced stability in the presence of water, which can downplay the positive impact on fuel advantages. U_3Si_2 gained much popularity for use for light-water reactors (LWR). Other experiments reported using a fuel made of beryllium oxide (BeO) combined with UO_2 matrix exhibited enhanced thermal conductivity, but with higher enrichment than UO_2 [5].

1.2. Spark Plasma Sintering

The sintering process of UO2 uses high temperatures of 1600–1750℃ with a hold time of approximately four hours, reaching a heating rate of 10 °C/min is acceptable. The SPS uses high pulsed currents to heat a conductive tooling assembly under simultaneous uniaxial pressure rapidly [6], [7]. The complete sintering cycle takes around ten hours, and it heats the ceramic fuel powder at half of the melting point, leading to fuel densification. Mixture powders graphite dies, next steps apply short-pulsed currents during hold time. During the current pulse, the fuel powder reaches the melting point. An application of 40 MPa of pressure ensures that powder particles become uniformly compacted. The SPS method can sinter carbon composite powder with 96% of theoretical density using temperatures of 1050 °C, with a hold time of 0.5 min, at a higher rate of the heat 200 °C/min [8]. In part, the process has many dependencies on powder preparation, grain size, and ceramic materials bought from different suppliers. There are a few sinter practices used to UO2 powder like the hot uniaxial pressing, but SPS can sinter fuels using carbon, such as UO2-SiC is like UO_2-diamond.

1.3. Composite Fuels with Carbon Compounds

Nuclear fuel suppliers will industrialize the SPS method, which can offer high-speed powder consolidation. SPS sintering techniques permit processing UO_2 composites, such as UO2 cermet that contains fractions of SiC, CNT, diamond powder, and Gd_2O_3 [9]. The fuel performance code FRAPCON simulated the UO_2-SiC composite fuel using a code version adapted to the composite material properties [10]. This investigation details the behavior of UO_2-CNT, and the addition of micro-diamond particles added to UO_2. All fuel carbon composites will significantly enhance the thermal conductivity of standard UO_2 fuel. There are experiments conducted with distributions of both multi-walled carbon nanotube (MWCNT) and single-walled carbon nanotube (SWNT). The mixture of UO_2 and CNTs can be sintered at 1300 ℃ with a hold time of 5 min and 40 MPa of pressure. These experiments reported pellet thermal conductivity improvements of 30%, with the addition of 5 vol% SWNT, compared with pure UO_2 values [11].

2.0 METHODS AND MATERIALS

2.1. Physical Properties of Composite Fuel

The first step consists of introducing full thermals and mechanical properties into the FRAPCON code to simulate fuel behavior under steady-state conditions. A lower thermal gradient will lead to a reduction in gaseous fission products, pellet-cladding interaction because of fuel cracking, relocation, and swelling. Rapid analysis of the physical properties of UO_2 and SiC appoints significant differences. Table 1 compares UO_2 and SiC at room temperature Morgan supplied that Advanced Ceramics, Rohm & Haas (Dow Chemical Company, U.S.), and COI Ceramics, Inc.

Table 1: Physical properties of UO_2 and SiC

Physical properties	SiC	UO_2
Bulk density (Kg/m^3)	2900-3210	10960
Thermal conductivity	250-300	8.68
Coefficient thermal expansion (μm/m)	2.2- 4.5	9.76
Specific heat (J/Kg-K)	640-670	235
Elastic modulus (MPa)	370-466	192
Poisson ratio	0.20	0.316

The thermal properties of SiC ceramics vary between different suppliers because of different manufacturing techniques, such as SiC-CVD and SiC-CVI.

SiC ceramics have desirable features, such as short half-life by neutron irradiation and considerable stability for severe neutron flux. SiC thermal conductivity is reasonably stable at temperatures upwards of 1546 °C to at least tens of displacement per atom (dpa). The Neutron fluence produces small Frank dislocation loops on crystal planes below 1000°C. Irradiation effects generate many tetrahedral voids at 1250 °C and 1500 °C that cause continuous swelling in SiC [12]. Equation 1 represents the standard relationship used to calculate the thermal conductivity of UO_2-SiC 10 vol%.

$$k = Cp \times \rho \times \alpha \quad (1)$$

where k is thermal conductivity (W/m-k), Cp is specific heat (J/kg-k), ρ is density (kg/m^3), and α is thermal diffusivity (m^2/s).

The thermal diffusivity of SiC can reach over 20 times that of UO_2 at temperatures below 1000°C. In this study, the fuel formulation under consideration is UO_2-SiC, which contains 10 vol% of SiC, with a theoretical density of 96.4%. The UO_2-SiC microstructure shows good bonding between the SiC and the UO_2 matrix. Table 2 lists the polynomial fit to the thermal diffusivity of UO_2 and SiC. Equation 2 shows polynomial coefficients used to calculate both chemical compounds SiCs and UO_2, valid from 300 K to the melting point of UO_2.

$$\alpha = A \times T^4 + B \times T^3 + C \times T^2 + D \times T + E \quad (2)$$

where T is the temperature is in K and α (m^2/s) is thermal diffusivity.

Table 2: Polynomial coefficients to thermal diffusivity of UO_2 and SiC

Compound	A	B	C	D	E
UO_2	2.5374×10^{-19}	-2.0952×10^{-15}	6.3611×10^{-12}	-8.6933×10^{-9}	5.273×10^{-6}
SiC	2.9827×10^{-17}	-2.1207×10^{-13}	5.4078×10^{-10}	-5.889×10^{-7}	2.4401×10^{-4}

2.2. Thermal conductivity of UO_2-SiC

SiC suppliers use various methods to produce SiC monolithic, and composite fibers generate different physical properties. Manufacture route show methods such as hot pressing, or sintering, silicon infiltrated silicon carbide (SiSiC). Another example is chemical vapor deposition and the production of single-crystal silicon. The thermal conductivity of UO_2-SiC sintered composite fuel shows a dependence on the amount of present dopant SiC powder. Thermal conductivity of the fuel must increase as the function of volume percent of SiC varies from a range of 5 to 20% vol. The thermal conductivity of the unirradiated UO_2 has a dependence on temperature. Equation 3 shows the relationship used, which considers the effects of porosity, irradiation, and fission products.

$$k(UO2)_{95} = \frac{100}{7.5408 + 17.692 \times Tn + 3.6142 \times Tn^2} + \frac{6400}{Tn^{5/2}} \exp\left(\frac{-16.35}{Tn}\right) \quad (3)$$

where Tn=(T(K)/1000), and $k(UO_2)_{95}$ is the thermal conductivity of 95% of the theoretical density of UO_2 in W/m-k.

Thermal conductivity models used to UO_2 expose dependence on deviation from stoichiometry, burnup, fractional porosity, and temperature. The conductivity loss of UO_2 for fission products that should increase due to phonon scattering. Equation 4 represents the thermal conductivity of UO_2 as a function of irradiation effects.

Equation 5 displays the correct thermal conductivity of irradiated UO_2 contains at least four correction parameters.

$$k(UO_2) = k(UO_2)_{95} \times \left(\frac{1}{1-(2.6-0.5Tn)\times 0.05} \right) \quad (4)$$

$$k = k(UO_2) \times FD \times FP \times FM \times FR \quad (5)$$

where *FD* is a factor for dissolved fission products, *FP* is a factor for precipitated fission products, *FM* represents the Maxwell factor to correct porosity effect, and *FR* represents the irradiation damage factor.

2.2.1 Hesselman and Johnson model

Several models measure the effective thermal conductivity of ceramic composites, where mixed materials are macroscopically homogenous [13]. Maxwell and Rayleigh were the first to write analytical expressions for effective conductivity. Eucken extended these expressions to allow for calculations with multiple phases. Next, arisen Hamilton-Crosser model, that expanded expressions by including the effects of different particle shapes. Figure 1 displays the thermal conductivity of UO_2 and SiC. The thermal conductivity specific heat of UO_2 shows discontinuity around 2000 K. The phase transition of UO_2 occur at a temperature about 2600 to 2700 K.

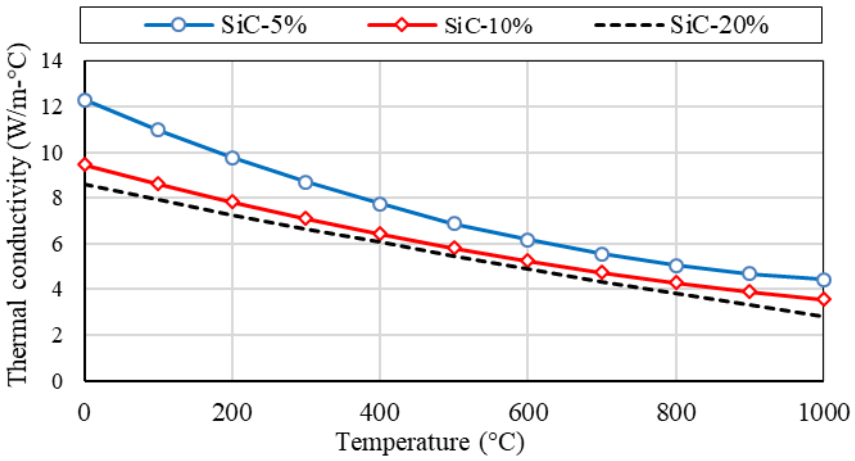

Figure 1: Thermal conductivity of composite UO_2-SiC, vol (5%, 10%, 20%)

The Hesselman-Johnson model (HJ) found a correlation for the thermal conductivity, widely used to nanoparticles, and interface regions between fiber and the host matrix, 1987. The UO_2-SiC show a thermal conductivity can provide a suitable agreement to the experimental data calculated with Hesselman-Johnson correlation. Equation 6 expresses the effective thermal conductivity of composites, according to the HJ model [14].

$$keff = k_{(UO_2)} \frac{\left(\frac{k(SiC)}{k(UO_2)} - \frac{k(SiC)}{rhc} - 1\right) Vf + \frac{k(SiC)}{k(UO_2)} + 2\frac{k(SiC)}{\alpha hc} + 2}{\left(1 - \frac{k(SiC)}{k(UO_2)} + \frac{k(SiC)}{rhc}\right) Vf + \frac{k(SiC)}{k(UO_2)} + 2\frac{k(SIC)}{\alpha hc} + 2} \quad (6)$$

where *Keff* represents the effective thermal conductivity, and $k_{(UO2)}$ is conductivity of UO_2 matrix, $k_{(SiC)}$ represents thermal conductivity of SiC used, *r* is the particle radius, and *hc* is the thermal conductance of the interface.

2.3. Thermal Expansion

Fresh fuel produced via SPS has several advantages, such as small grain sizes, higher theoretical density, and enhanced thermal conductivity. Therefore, fuel pellets sintering following Vegard's law, the thermal expansion results from a function of contents. The ceramics have a low linear thermal expansion coefficient of about 4 µm/m°C compared with UO_2 at 9.76 µm/m°C. The linear thermal expansion of SiC is a function of temperature described with a polynomial correlation. Figure 2 illustrates the temperature expansion coefficients of the UO_2 and SiC.

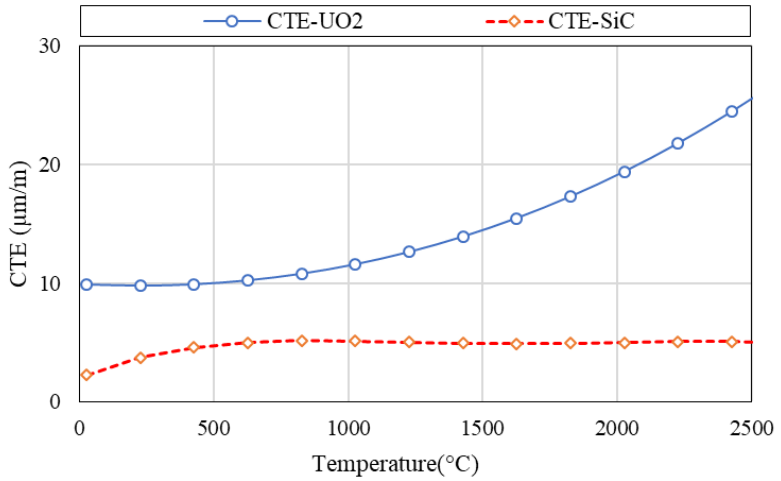

Figure 2: Thermal expansion coefficients of UO_2 and SiC.

2.4 Heat Capacity

UO_2 with 10 vol% SiC has a higher heat capacity than UO_2 when calculated by combining the weight fraction of all contents and multiplying by a single heat capacity of both UO_2 and SiC, as shown in Eq. 7.

$$Cp_{(UO_2 - SiC)} = W_{(UO_2)} \times Cp_{(UO_2)} + W_{SiC} \times Cp_{(SiC)} \quad (7)$$

In the formula, it converts volume fraction to weight fraction. Next, it needs a relationship between the heat capacities of UO_2 and to calculate the heat capacity of UO_2-SiC. The heat capacity for solid UO_2 is a function of temperature, fuel composition, and the oxygen-to-metal ratio. Equation 8 displays the specific heat capacity of pure UO_2.

$$Cp_{(UO_2)} = \frac{K_1\theta^2 \exp(\theta/T)}{T^2[\exp(\theta/T)-1]^2} + K_2T + \left(\frac{O/M}{2}\right)\frac{K_3E_D}{RT^2}\exp(-E_D/RT) \quad (8)$$

where *Cp(UO2)* is specific heat capacity (J/kg-K), K_1=296.7, K_2=2.43×10^{-2}, K_3=8.745×10^7, R is the universal gas constant 8.3143 J/mol-K, θ=535.285 represents the Einstein temperature, and ED=1.577×10^6 means the activation energy for Frenkel defects (J/mol).

The correlation adopted to the specific heat of SiC increases slowly with increasing temperatures above 73.15°C. Equation 9 shows the heat capacity of SiC and SiC with temperature dependence. Figure 3 displays heat capacities as a function of temperature for UO_2 and SiC.

$$Cp(SiC) = 925.65 + 0.3772 \times T - 7.9259 \times 10^{-5}T^2 - \frac{3.1946 \times 10^7}{T^2} \quad (9)$$

where T represents the temperature in K. The uncertainties reach ± 7% below 726.85°C and ± 4% from 726.85 °C to 2126.85 °C.

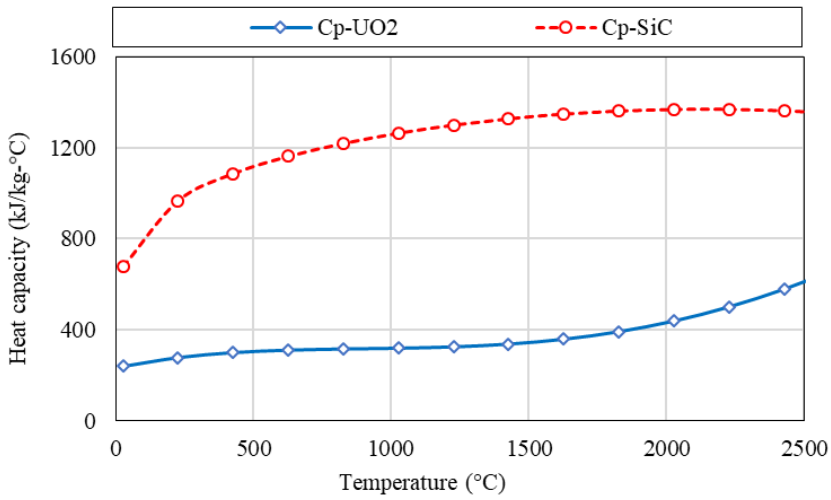

Figure 3: Specific heat as a function of temperature for UO_2 and SiC.

2.5. Mechanical Models

In this study, models of UO_2 creep, fuel cracking, and relocation could investigate the behavior of UO_2-SiC 10% vol fuel. It expects these models to show a better response to the creep rate of composite fuel when using the spark plasma sintering method because of the reduced weight fraction of silicon and carbon in the sintered pellet. The simulation used the swelling model of

UO_2 and the behavioral of UO_2-SiC Equation 10 displays solid fission product as a simple linear function of burnup. Equation 11 expresses the swelling gaseous fission products that are a semi-empirical model for UO_2 fuel. Computational simulations promoted based on multi-physics modeling for UO_2-SiC fuels appointed to a lower fission gas release in comparison with UO_2.

$$\Delta(sw-s) = 5.577\times10^{-5}\rho\Delta Bu \tag{10}$$

where *Δ(sw-s)* represents the solid swelling increment, ΔBu the burnup increment uranium fissions, and *r* is the density (kg/m^3).

$$\Delta\varepsilon_{(sw-g)} = 1.96\times10^{-31}\rho\Delta Bu(2800-T)^{11.73} * e^{-0.0162(2800-T)} * e^{-0.0178\rho Bu} \tag{11}$$

where *Δ(sw-g)* expresses the gaseous swelling increment, *ΔBu* the burnup increment uranium fissions, and *r* is the density (kg/m^3), and *T* is the temperature in K. Gaseous swelling become relevant above 1500 K.

2.6. Elasticity Behavior

The effects of temperature observed on the modulus of elasticity of polycrystalline solids expose a linear relationship, decreasing with increasing temperature. UO_2 has a modulus of elasticity of 200 ± 20 GPa at room temperature. The elastic response, at temperatures near the melting point, decreases more rapidly than linear extrapolation because of stress relaxation at grain boundaries. Equation 12 shows the modulus of elasticity of UO_2. Figure 4 illustrates the modulus of elasticity of the materials investigated [15], [17], [18].

$$E_{(UO2)} = 2.334\times10^{11}(1-2.752(1-D))(1-1.0915\times10^{-4}T) \tag{12}$$

where *T* is K, and *D* is the porosity of the pellet, assumed to be 0.05%

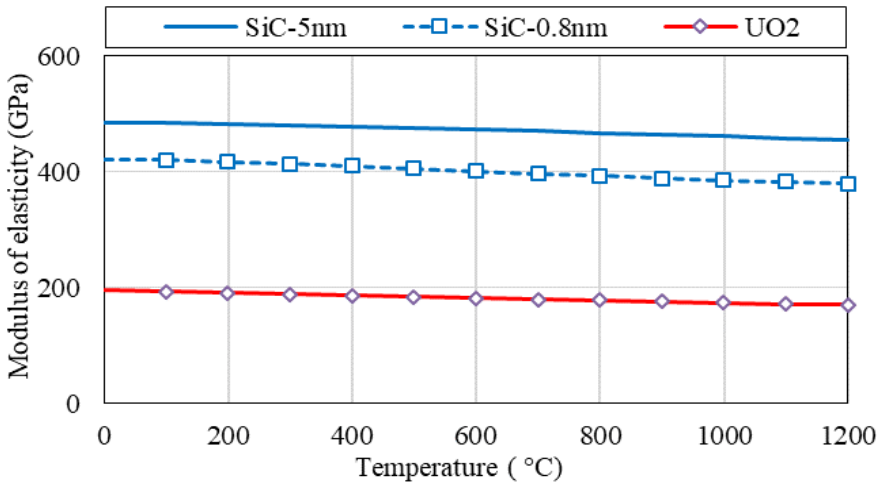

Figure 4: Modulus of elasticity of 3C-SiC and UO_2.

The elasticity of SiC is higher than iron alloys on the temperature range of interest. Mechanical response from 25 C appoints that Zr-4 exhibits values of 99.3 GPa, while alpha-SIC showed 410 GPa and SIC-CVD exhibit 420 GPa.

3. RESULTS

The purpose of this study was to compare the thermal fuel response from UO_2 and composite sintered UO_2-SiC 10 vol%. The reactor used in simulations is PWR 17x17 with 4-Loop core is consists of 193 fuel assemblies. Table 3 compiles the fuel properties defined on the input files of the FRAPCON code.

Table 3: PWR fuel properties used as inputs to FRAPCON code

PWR fuel parameters	Nominal values
Pellet outer diameter (mm)	8.19
Pellet length (mm)	9.83
Pellet density (% of theoretical)	95.50
Rod pitch (mm)	12.60
Cladding outer diameter (mm)	9.50
Cladding wall thickness (mm)	0.57
Diametral gap (μm)	165.10
Active rod length (m)	365.76

Core design support around 118.3 tonnes of UO_2, and 28.7 tonnes of zircalloy. The fuel characteristic used in the simulation came from fuel suppliers. Figure 5 illustrates the axial power profile used during the irradiation cycle.

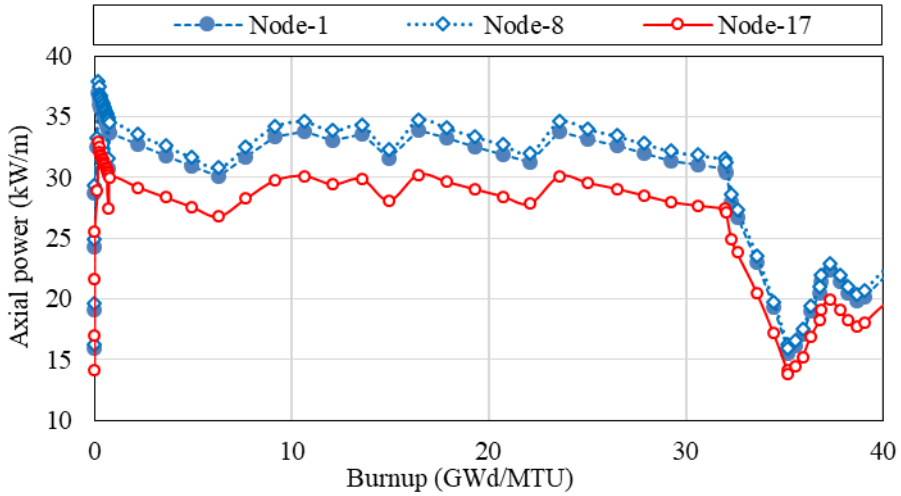

Figure 5: Power in axial nodes with two at the extremes and the central node

The number of fresh fuel assemblies reloaded during each outage is 84, matching well with the current industrial practice. The core design planned to a cycle length of 18 months and

reactivity coefficients to operate at 3587 MWth. The core design uses 264 fuel rods and 25 guide tube channels for control rods and instrument tubes. The PWR shows a fuel enrichment grading pattern that works with three regions graded at 2.35%, 3.40% and 4.445% of U-235. The proposed fuel option shows enhanced thermal conductivity and a high melting point while exhibiting low neutron absorption and acceptable radiation resistance attributed to SPS sintering. The temperature in the centerline of a fuel pellet is a function of the linear power rate and thermal conductivity of the selected fuel.

The complete burnup cycle performed was 685 effective power days, and the linear heat rate used was 30.457 kW/m. The total power produced reached 40.84 GWd/MTU, with a maximum centerline temperature of 1140 °C and 8.11% fission products. Table 4 exhibits a simple comparison from fuel response using FRAPCON code original version for UO_2, and an adapted version for UO_2-15%SiC

Table 4: Parameters used in the simulation of the commercial type reactor PWR 17x17

Parameters of operations	UO_2	UO_2-15%SiC
Effective power days (days)	685	685
Burnup discharged (GWd/MTU)	50.20	53.54
Hydrogen uptake (ppm)	224	222
Fission gas release (%)	3.87	2.72

A PWR fuel rod showed burnup discharged of 58 (GWd/MTU) under a short cycle of 656 effective power days. The fuel rod length of 3.65 using zircaloy as cladding. The outer diameter was 9.50 mm, and the wall thickness was 0.75 mm, and yielding a plenum volume of 18.60 cm^3. The gap filled as He pressurized at 4 MPa. Figure 6 shows a comparison of the fuel centerline temperature between UO_2 and UO_2-SiC 10 and 15 vol%.

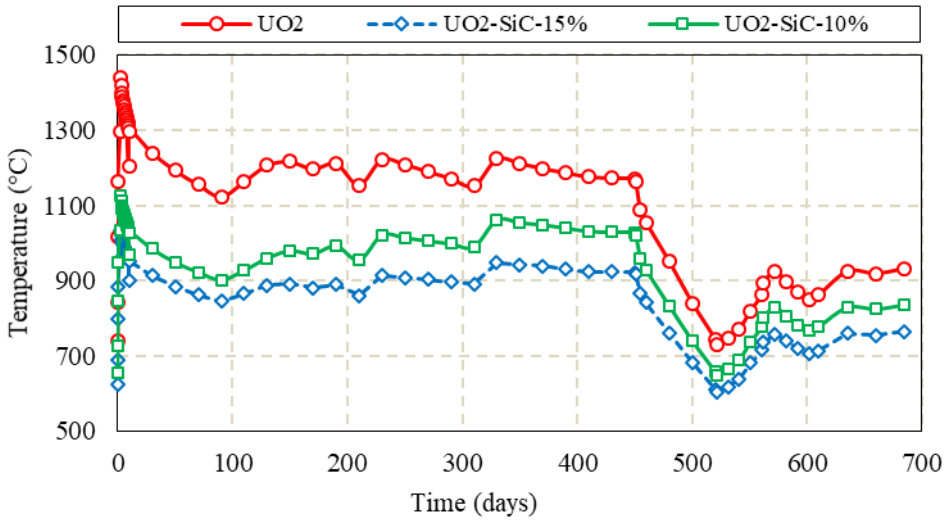

Figure 6: Comparison of fuel centerline temperature.

Rod internal pressure is a safety criterion used to measure the life-limiting factor for nuclear fuel. The plenum pressure model changes the internal pressure for each time-step. The model

used to determine plenum pressure includes moles fraction contained between the fuel and cladding. Figure 7 illustrates the fuel rod plenum pressure during the irradiation cycle.

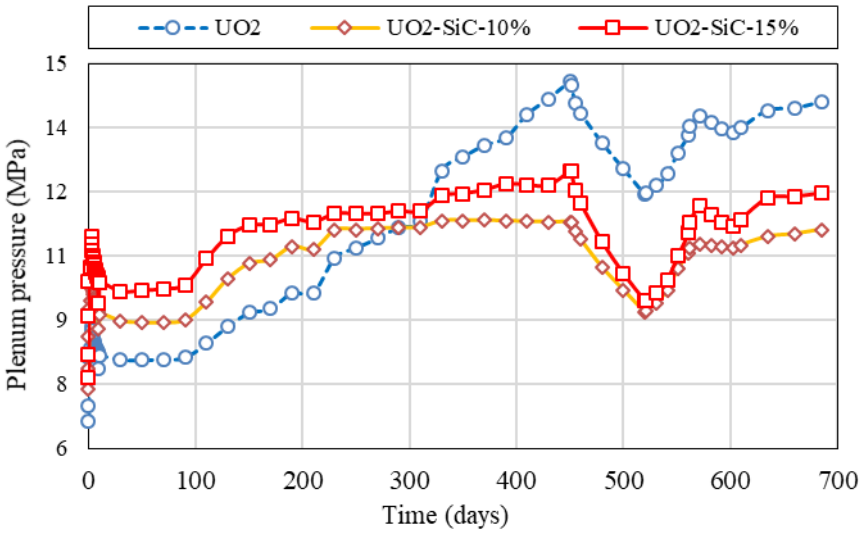

Figure 7: Fuel rod plenum pressure using UO_2 and UO_2-SiC 10 and 15 vol%.

The linear heat rate is the most critical parameter for controlling gaseous fission products. The enhanced thermal conductivity of SiC additions in a UO_2 matrix reduced thermal gradients into fuel pellets.

Practical observations consider that the gaseous products are Xe and Kr, which reach less than 1% fission gas release (FGR) at rates between 20 to 25 kW/m. Therefore, SiC addition with higher conductivity and chemical contents reduced the FGR rates. Figure 8 illustrates the fission gas release during the burn cycle.

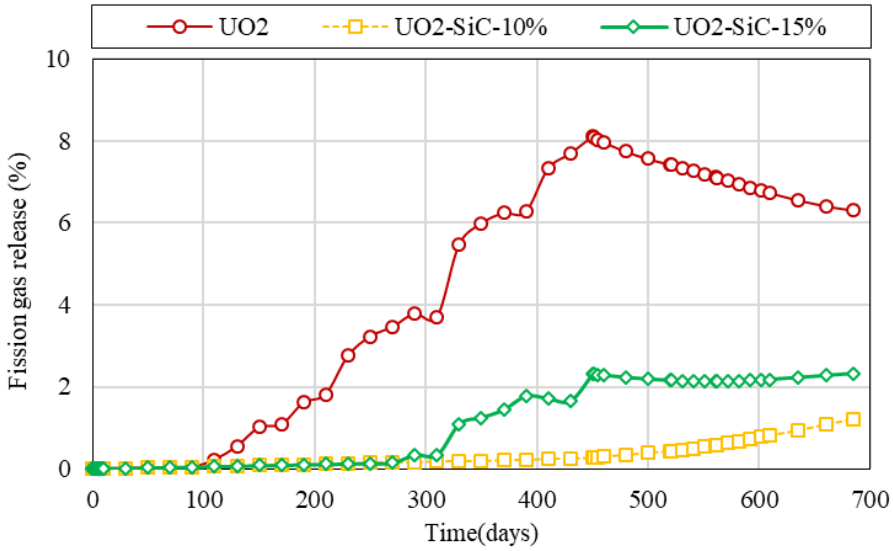

Figure 8: Fission gas release of UO_2 and UO_2-SiC 10 and 15 vol%.

During the burn cycle, the gap size decrease then creates solid contact between the pellet fuel and the cladding wall. The mechanical contact starts fuel relocation. Also, hard contact establishes a pellet mechanical interaction. Extended effects are the chemical contact that promotes stress corrosion cracking. Figure 9 shows the gap closures of UO_2-SiC and UO_2.

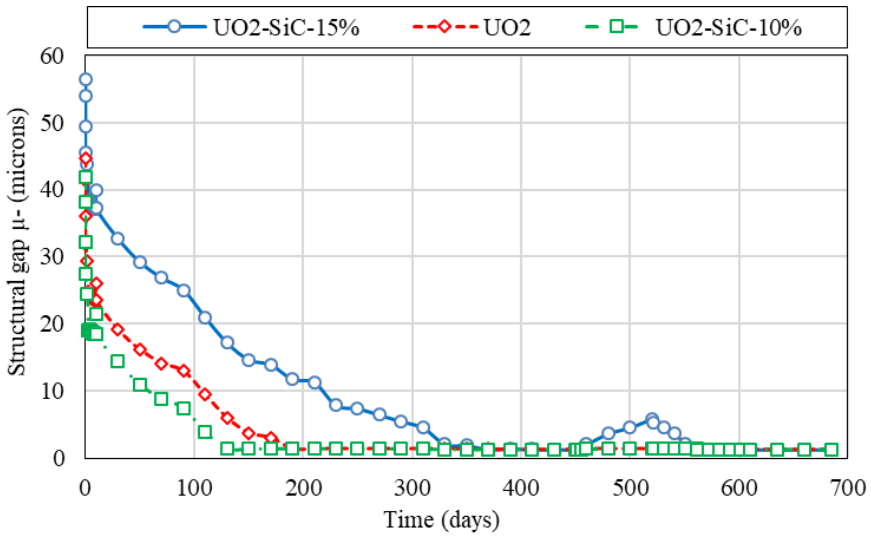

Figure 9: Gap closure process using UO_2-SIC

Pellet–cladding mechanical interaction (PCMI) is the most persistent and troublesome phenomena that can produce failures in the cladding. During regular operation, irradiated UO_2 pellets must expand thermally and distort from a cylindrical to an hourglass shape, with convex ends. The interaction can also occur during power ramps. Mechanical contact intensifies fuel cracking and particle relocation.

4. CONCLUSION

The chemical compatibility of SiC with UO_2 fuels are of great importance and offers many advantages in nuclear applications. Silicon carbide shows reduced gaseous diffusion coefficients, but gaseous diffusions are always possible because of structural imperfections. Regarding mechanical properties, SiC-CVD exhibits a higher elastic modulus of 420 GPa, flexural strength, bi-axial strength, and an enhanced creep rate.

Therefore, during an extended irradiation cycle had the plutonium formation on UO_2 fuel occurs near the outer surface of the fuel, or RIM region. This is because plutonium formation induces a restructuring process, creating a high burnup structure (HBS) in part because of epithermal U-238 resonance absorption. Especially at the outer border of the pellet, large UO_2 grains disintegrate into a nanosized particle regrettably, the physical models of the formation of the HBS [8]. Therefore, the model uses a non-conventional sintering practices, known as high-pressure spark plasma sintering (HP-SPS). The SPS methods have many advantages over traditional UO_2 sintering methods, and it can reduce HBS formation or RIM regions with more severe crystal damage. This process produces a rapid consolidation of the composite powder, creating a highly dense microstructure, and allowing minimum grain growth using low temperatures.

Actual results of SPS are attractive to application for the large-scale production of nuclear ceramic fuel.

ACKNOWLEDGMENTS

The authors are very grateful for the support received from the Nuclear Energy Research Institute (IPEN), in association with the Brazilian government agency, National Nuclear Energy Commission (CNEN).

REFERENCES

1. T. Barani, G. Pastore, D. Pizzocri, D. A. Andersson, C. Matthews, A., Alfonsi, J., D., Hales, "Multiscale modeling of fission gas behavior in U3Si2 under LWR conditions". *Journal of Nuclear Materials*, **Vol. 522**, pp. 97-110 (2019).
2. A. K. Singh, S. C., Zunjarrao, R. P. Singh, "Silicon carbide and uranium oxide-based composite fuel preparation using polymer infiltration and pyrolysis." *In 14th International Conference on Nuclear Engineering* American Society of Mechanical Engineers, pp. 427-433) (2006).
3. S. Yeo, E. Mckenna, R. Baney, G. Subhash, J. Tulenko, "Enhanced thermal conductivity of uranium dioxide–silicon carbide composite fuel pellets prepared by Spark Plasma Sintering (SPS)." *Journal of Nuclear Materials*, **Vol. 433(1-3),** pp. 66-73 (2013).
4. Z. Chen, G. Subhash, J. J. Tulenko, "Master sintering curves for UO2 and UO2–SiC composite processed by spark plasma sintering". *Journal of Nuclear Materials*, **Vol. 454(1-3)**, pp. 427-433 (2014).
5. S. Chen, C. Yuan, "Neutronic analysis on potential accident tolerant fuel-cladding combin ation U3Si2-FeCrAl". *Science and Technology of Nuclear Installations,* **Vol. 2017**, pp.16 (2017)
6. W. Zhou, R. Liu, S. T. Revankar, "Fabrication methods, and thermal hydraulics analysis of enhanced thermal conductivity UO2–BeO fuel in light water reactors". *Annals of Nuclear Energy*, **Vol. 81**, pp. 240-248 (2015).
7. A. Cartas, H. Wang, G. Subhash, R. Baney, J. Tulenko, "Influence of carbon nanotube dis persion in UO2–carbon nanotube-ceramic matrix composites utilizing spark plasma sinter ing". *Nuclear Technology,* **Vol. 189(3),** pp. 258-267 (2015)
8. V. Tyrpekl, M. Cologna, J. F. Vigier, A. Cambriani, W. De Weerd, J. Somers, "Preparation of bulk-nanostructured UO2 pellets using high-pressure spark plasma sintering for LWR fuel safety assessment". *Journal of the American Ceramic Society*, **Vol. 100(4)**, pp. 1269-1274 (2017).
9. T. Wiss, V. V. Rondinella, R. J. Konings, D. Staicu, D. Papaioannou, S. S. Bremier, A. Schubert, "Properties of the high burnup structure in nuclear light water reactor fuel." *Radiochimica Acta,* **Vol. 105(11),** pp. 893-906 (2017).
10. R. Liu, W. Zhou, A. Prudil, P. K. Chan, "Multiphysics modeling of UO2-SiC composite fuel performance with enhanced thermal and mechanical properties". *Applied Thermal Engineering*, **Vol. 107**, pp. 86-100 (2016)].
11. K. J. Geelhood, W. G. Luscher, *FRAPCON-4.0: integral assessment*. PNNL-19418, **Vol. 1, 2** (2015).

12. W. Zhou, W. Zhou, “Enhanced thermal conductivity accident tolerant fuels for improved reactor safety–A comprehensive review." *Annals of Nuclear Energy*, **Vol. 119**, pp. 66-86, (2018).
13. M. I. Idris, H. Konishi, M. Imai, K. Yoshida, T. Yano, “Neutron irradiation swelling of SiC and SiCf/SiC for advanced nuclear applications." Energy Procedia, **Vol. 71**, pp. 328-336 (2015).
14. L. F. Johnson, D. P. H. Hasselman, E. Minford, “Thermal diffusivity and conductivity of a carbon fiber-reinforced borosilicate glass.” *Journal of Materials Science*, **Vol. 22(9)**, pp. 3111-3117 (1987).
15. K. Pietrak, T.S. Wiśniewski, “A review of models for effective thermal conductivity of composite materials." *Journal of Power Technologies*, **Vol. 95(1),** pp. 14-24 (2014).
16. W. X. Wang, L. S. Niu, Y. Y. Zhang, E. Q. Lin, E. Q. “Tensile mechanical behaviors of cubic silicon carbide thin films." *Computational Materials Science,* **Vol. 62**, pp. 195-202 (2012).